Nanoscale Res Lett (2008) 3:186–193
DOI 10.1007/s11671-008-9134-4

NANO EXPRESS

Surface Morphological and Nanomechanical Properties of PLD-Derived ZnO Thin Films

Sheng-Rui Jian · I-Ju Teng · Ping-Feng Yang · Yi-Shao Lai · Jian-Ming Lu · Jee-Gong Chang · Shin-Pon Ju

Received: 11 December 2007 / Accepted: 7 May 2008 / Published online: 21 May 2008

Abstract This study reports the surface roughness and nanomechanical characteristics of ZnO thin films deposited on the various substrates, obtained by means of atomic force microscopy (AFM), nanoindentation and nanoscratch techniques. ZnO thin films are deposited on (a- and c-axis) sapphires and (0001) 6H-SiC substrates by using the pulsed-laser depositions (PLD) system. Continuous stiffness measurements (CSM) technique is used in the nanoindentation tests to determine the hardness and Young's modulus of ZnO thin films. The importance of the ratio (H/E_{film}) of elastic to plastic deformation during nanoindentation of ZnO thin films on their behaviors in contact-induced damage during fabrication of ZnO-based devices is considered. In addition, the friction coefficient of ZnO thin films is also presented here.

S.-R. Jian (✉)
Department of Materials Science and Engineering, I-Shou University, Kaohsiung 840, Taiwan, ROC
e-mail: srjian@gmail.com

I.-J. Teng
Department of Materials Science and Engineering, National Chiao Tung University, Hsinchu 300, Taiwan, ROC

P.-F. Yang · Y.-S. Lai
Central Labs, Advanced Semiconductor Engineering, Kaohsiung 811, Taiwan, ROC

J.-M. Lu · J.-G. Chang
National Center for High-Performance Computing, National Applied Research Laboratories, No. 28, Nanke 3rd Rd., Sinshih Township, Tainan County 74147, Taiwan, ROC

S.-P. Ju
Department of Mechanical and Electro-Mechanical Engineering; Center for Nanoscience and Nanotechnology, National Sun-Yat-Sen University, Kaohsiung 804, Taiwan, ROC

Keywords ZnO · PLD · AFM · Nanoindentation · Nanoscratch · Hardness

Introduction

ZnO semiconductor, having a wide direct band gap of 3.37 eV at room temperature, has attracted much attention because of its wide applications in various optoelectronic and electronic devices. In addition, it has been considered as a prime candidate for ultraviolet light emitting diodes and lasers due to its larger exciton binding energy of 60 meV [1, 2]. In contrast, research on the mechanical properties has not drawn equal attention. The successful fabrication of devices based on ZnO thin films requires an understanding of the mechanical characteristics in addition to its optical and electrical performances. Due to the contact loading during processing or application, the performances of these devices can be significantly degraded. It is of interest to investigate the mechanical characteristics of materials at nanoscale for device applications.

The mechanical characteristics of materials are size-dependent. Thin films may have different mechanical responses from their bulk materials. Until recently, the role of structural changes under contact loading was largely underestimated owing to the difficulties in structural characterizations of thin films affected by the contact interaction. Nanoindentation is an instrumented depth-sensing technique that has enabled the measurement of mechanical properties from small volumes of materials and thin films. Such mechanical properties, e.g., hardness and elastic modulus, can be determined directly from indentation load versus displacement curves [3–6]. In fact, the load-displacement curves obtained during nanoindentation can be viewed as "fingerprints" that contain much

information about deformation mechanisms [7–9]. It appears meaningful to extend the nanoindentation study to the ZnO thin films, in merit of both basic research and technological applications. In addition, nanoscratch technique can be used to characterize the nanotribological properties of ZnO thin films by scratching the ZnO surface using a diamond tip and recording the coefficient of friction, in situ scratch depth and residual depth. However, although nanoscratch technique has been widely used to evaluate the nanotribological properties of metallic, ceramic, and polymeric thin films materials [10–12], to our knowledge, much less attention has been done on ZnO thin films.

Herein, the purpose of the present work is to report on the results of experiments designed to prepare ZnO thin films on various substrates by using a pulsed-laser deposition (PLD) system and, to investigate the surface morphological and mechanical behaviors of ZnO thin films by using atomic force microscopy (AFM) and nanoindentation/nanoscratch techniques, respectively, with particular reference to the effects of substrates on mechanical properties of thin films/substrates systems.

Experimental Details

The Growth Conditions of ZnO Thin Films

ZnO thin films were grown on (0001) (c-oriented), $(11\bar{2}0)$ (a-oriented) sapphire and (0001) 6H-SiC substrates by using PLD system, which is popularly adapted in growing ZnO layers [13, 14]. A KrF excimer laser (Lambda physik 210, $\lambda = 248$ nm) is employed and the beam was focused to produce an energy density of $\sim$ 5–7 J/cm^2 with 10 Hz repetition rate at a 45^{o} angle of incidence on a commercial hot pressed stoichiometric ZnO (99.99% purity) target. The thin films were deposited at $\sim$ 0.625 Å/sec growth rate at 600 °C substrate temperature under base vacuum of 3.5×10^{-9} torrs, and then in-situ annealed at 700 °C for 1 h. No oxygen gas flow was introduced during the growth and annealing. In all cases, the ZnO epilayers are $\sim$ 600 nm thick.

Surface Features Characterizations

Samples are imaged at room temperature using a commercial atomic force microscopy (AFM, Nanoscope III, Digital Instruments) equipped with soft (version 4.32) for images processing and roughness calculation. For tapping mode we used rectangular silicon cantilevers (nanosensors, 125 μm long, 30 μm wide and 4 μm thick) with a tip radius of about 10 nm, a normal spring constant of 40 N/m and resonance frequency of 339 kHz.

The surface roughness can be represented by center line average (R_a) and root-mean-square average (*RMS*) [15] in the following forms:

$$R_a = \frac{1}{n}\sum_{i=1}^{n}|z_i|, \tag{1}$$

$$RMS = \sqrt{\frac{1}{n}\sum_{i=1}^{n}z_i^2}. \tag{2}$$

The center line is the line that divides the profile in such a way such that the net deviation is zero. Both R_a and *RMS* measure the average vertical deviation of surface profile from the center line. It should be noted that these parameters can only be used to compare sample surfaces generated by the same method in Ref. [16].

Nanoindentation and Nanoscratch Measurements

The nanoindentation measurements were performed on a Nanoindenter MTS NanoXP® system (MTS Cooperation, Nano Instruments Innovation Center, TN, USA) with a diamond pyramid-shaped Berkovich-type indenter tip, whose radius of curvature is 50 nm. The mechanical properties (the hardness and Young's modulus) of ZnO thin films were measured by nanoindentation with a continuous stiffness measurements (CSM) technique [17]. In this technique, a small sinusoidal load with known frequency and amplitude was superimposed onto the quasi-static load. It results in a modulation of the indenter displacement that is phase shifted in response to the excitation force. The stiffness, S, of the material, and the damping, wC, along indentation loading can be respectively calculated using Eqs. 3 and 4 expressed below. The hardness and elastic modulus are, then, calculated by putting the obtained stiffness data into Eqs. 5–7, respectively. In this way, the hardness (H) and reduced elastic modulus (E_r) as a function of penetration depth are determined for a single loading/unloading cycle [18].

$$S = \left[\frac{1}{\frac{P_{\max}}{h(w)}\cos\Phi - (K_s - mw^2)} - K_f^{-1}\right]^{-1} \tag{3}$$

$$wC = \frac{P_0}{h(w)}\sin\Phi \tag{4}$$

$$H = \frac{P_{\max}}{A_c} \tag{5}$$

$$S = 2E_r h_c\sqrt{\frac{A_c}{\pi}} \tag{6}$$

$$\frac{1}{E_r} = \frac{\left(1 - v_{\text{film}}^2\right)}{E_{\text{film}}} + \frac{\left(1 - v_i^2\right)}{E_i} \tag{7}$$

where $P_{\max}$ and $h(w)$ are denoted as the driving force and the displacement response of the indenter, respectively; Φ is the phase angle between $P_{\max}$ and $h(w)$; m is the mass of the indenter column; K_s is spring constant at the vertical direction; K_f is frame stiffness; m, K_s and K_f are all constant values for specified indentation system; w is angular speed which equals to $2\pi f$; f is the driven frequency of the ac signal of 45 Hz for this work, which is used to avoid the sensitivity to thermal drift; the loading resolution of the system was 50 nN; and A_c is contact area when the material in contact with indenter being loaded at $P_{\max}$. E_{film} and v_{film} are elastic modulus and Poisson's ratio for thin films and, E_i (= 1,141 GPa) and v_i (= 0.07) are the same parameters for a indenter. Here, v_{film} is set to be 0.25 [19] for current analysis.

The area function, which is used to calculate contact area, A_c, was carefully calibrated by using fused silica as the standard sample prior to the nanoindentation experiments. The nanoindentation tests were carried out in the following sequence: first of all, the Berkovich indenter was brought into contact with the surface at a constant strain rate of 0.05 s^{-1}. The load was then held at the maximum value for 30 s in order to determine the creep behavior. The Berkovich indenter was then withdrawn from the surface at the same rate until 10% of the maximum load was reached. This constant strain rate was chosen such that the strain-hardening effect can be avoided during the measurements. And, at least 10 indents were performed on ZnO thin films. The nanoindentations were sufficiently spaced to prevent from mutual interactions.

Scratch testing was measured using a Nano Indenter XP® system with options for lateral-force measurements. The procedure was similar that presented in detail elsewhere [20]. The normal indenter load was linearly ramped from the minimum to maximum (0–5 mN) during the scratching. The translation speed was typically 50 μm/s. The test was repeated four times for each system. The average values of the coefficient of friction (μ) of four scratched at the same maximum constant normal load was used to estimate the friction behavior of the samples. After scratching, the wear tracks were imaged by AFM.

Results and Discussion

Surface Features

Typical AFM images of ZnO thin films deposited on the three substrates of a-axis sapphire, c-axis sapphire, and (0001) 6H-SiC, respectively, are presented in Fig. 1, where the island-like surfaces are clearly visible. From AFM observations, R_a and *RMS* for each specimen are accurately obtained. Moreover, mechanical characteristics by nano-indentation are prerequisite to perform under allowably

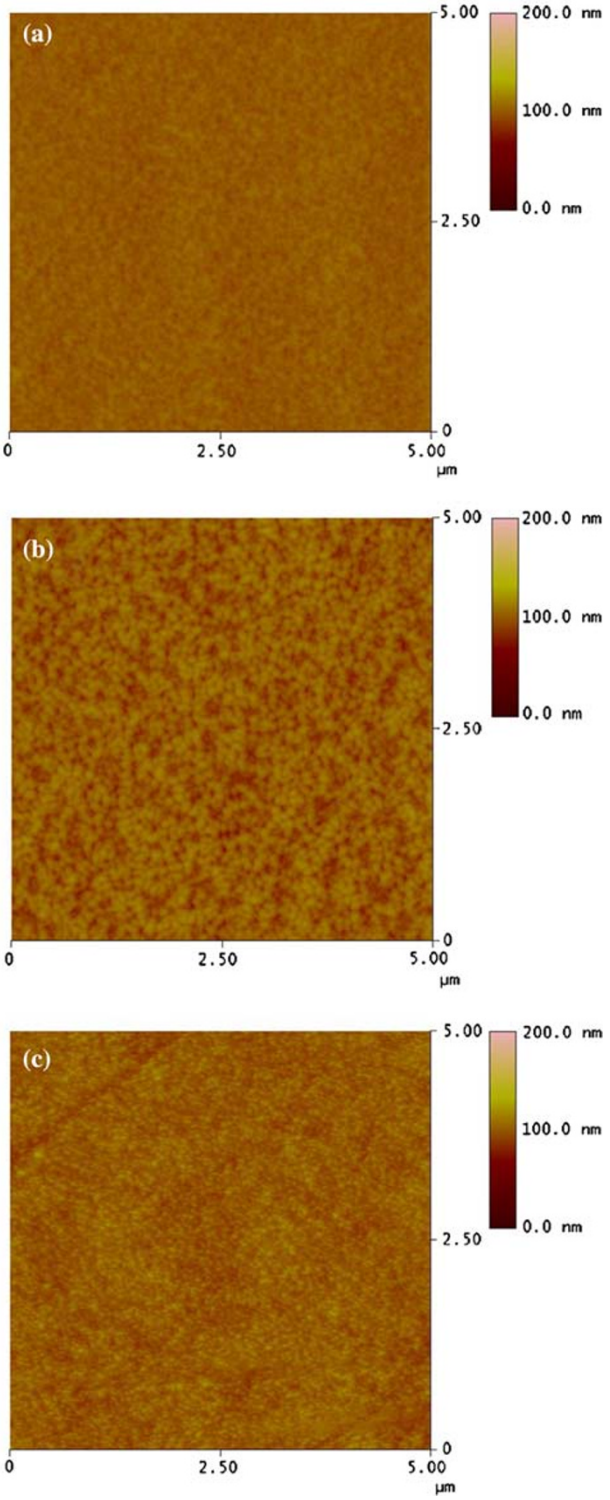

Fig. 1 AFM images of ZnO thin films deposited on the various substrates for (**a**) a-axis sapphire, (**b**) c-axis sapphire, and (**c**) (0001) 6H-SiC, respectively

Table 1 The surface roughness and evaluated mechanical properties of ZnO thin films and bulk materials (S.-R. Jian* et al.)

	ZnO fiilm/sapphire	ZnO film/c-sapphire	ZnO films/(0001) 6H-SiC	ZnO films	ZnO (bulk)
R_a	2.3 nm*	3.6 nm*	4.1 nm*		
RMS	2.8 nm*	4.5 nm*	5.2 nm*	13.5–20.6 nm [19]	
H	11.5 ± 0.8 GPa*	7.4 ± 0.1 GPa*	5.9 ± 0.2 GPa*	9.2 ± 0.810.4 ± 0.4 GPa [19]	2.2 ± 0.2 GPa (a-oriented bulk) [27]
	6.6 ± 1.2 GPa [27]	5.7 ± 0.8 GPa [27]		9.3–12.1 GPa [28]	4.8 ± 0.2 GPa (c-oriented bulk) [27]
				8.7 ± 0.2 GPa [29]	
E_{film}	212.2 ± 0.1 GPa*	150.1 ± 5.7 GPa*	117.1 ± 0.4 GPa*	9.2 ± 0.8–10.4 ± 0.4 GPa [19]	163 ± 6 GPa (a-orientedbulk) [27]
	318.2 ± 50 GPa [27]	310.1 ± 40 GPa [27]		103.5–114.4 GPa [28]	143 ± 6 GPa (c-oriented bulk) [27]
				154 ± 5 GPa [29]	
H/E_{film}	0.054 ± 0.004*	0.050 ± 0.002*	0.049 ± 0.001*		
μ	0.25 ± 0.02*	0.28 ± 0.01*	0.31 ± 0.02*		

* The present study

smooth surface for specimen requirement and allowable thermal drift for environmental control, following that convergent curves of hardness and modulus are obtained. R_a and *RMS* of ZnO thin films deposited on a-sapphire substrate are presented the smaller value while its crystal structure is closely arranged. In addition, the R_a and *RMS* of ZnO thin films were summarized in Table 1.

Nanoindentation Analysis

The typical indentation load-displacement curves of all ZnO thin films are shown in Fig. 2(a). Of note, there is no manifestly "pop-in" event displayed in the loading part of all load-displacement curves of ZnO thin films. The phenomena are very different from the previous studies [21, 22], which display the multiple "pop-ins" in single-crystal (wurtzite) ZnO.

The physical mechanisms of the multiple "pop-ins" appearing in the load-displacement curve have been extensively discussed in the literatures. Among all, crack formation [23], sudden occurrence of pressure-induced phase transformation [24] and, generation of slip bands because of dislocation propagation [9] during the nanoindentation process were identified to have occurred in the different systems. In contrast, epitaxial layers are expected to contain more defects like surface steps [25] that are known to facilitate the onset of plasticity [26]. In addition, this may be due, in part; pop-in events were attributed to the very poor defect density prior to the nanoindentation tests so that the onset of plasticity requires load sufficient for dislocation nucleation and propagation. In fact, during this research, no pop-in events are observed.

The displacement dependence of the hardness and Young's modulus of ZnO thin films can be obtained because of the CSM measurements, as illustrated in Fig. 2(b, c). As displayed in Table 1, which summarizes the hardness and Young's modulus for various ZnO samples obtained from different indentation methods [19, 27–29], the values obtained by using Berkovich indenter are somewhat larger than those obtained by other methods. In 2004, Li et al. [30] proposed that the nanoindentation depth should never exceed 30% of films thickness. From the presented results, it can be observed that the sudden drop over the same range of indentation depth (from 40 nm to 100 nm) wherein the softening occurs and remains relatively constant. That is, no manifestly substrate effect is displayed here. Thereby, we can speculate that the discrepancies among the mechanical properties of ZnO thin films are reasonably explained by the various growth environments of thin films, the indentation instruments and operational conditions.

Fig. 2(b) displays the hardness of ZnO thin films calculated by using the method of Oliver and Pharr [18]. The plot can be divided into two stages, namely, increase and decrease to constant. The hardness is observed to increase with increasing the penetration depth at small depth. The increase in hardness at small penetration depth is usually attributed to the transition between purely elastic to elastic/plastic contact whereby the hardness is really the mean contact pressure. Only under a condition of a fully developed plastic zone does the mean contact pressure represent the hardness. When there is no plastic zone, or a partially formed plastic zone, the mean contact pressure (which is measured using the Oliver and Pharr method) is less than the nominal hardness. After the first stage, the hardness decreases to constant stage and reaches constant values of ZnO thin films on three various substrates, as listed in Table 1, respectively. The constant characteristic of

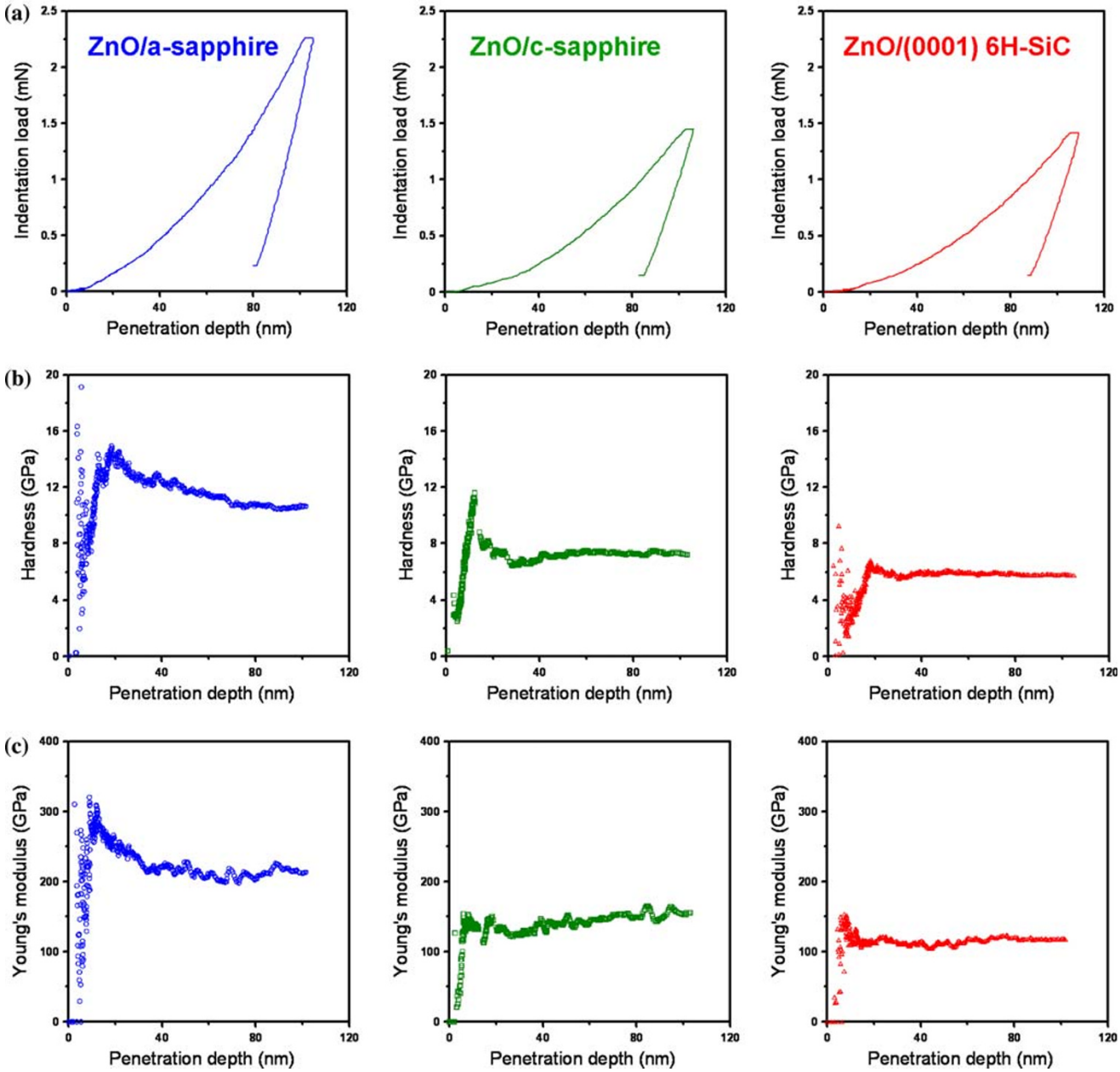

Fig. 2 Nanoindentation test results: (**a**) the typical load-displacement curves for ZnO thin film deposited on the various substrates; (**b**) hardness-displacement curves, and (**c**) Young's modulus-displacement curves for ZnO thin films

hardness is consistent with that of a single material; therefore, the hardness values at this stage could be regarded as film-only properties. In addition, a plot of Young's modulus of ZnO thin films on three various substrates determined using the method of Oliver and Pharr [18] is illustrated in Fig. 2(c). The variation of results is similar to those illustrating in Fig. 2(b); corresponding to the tendency of increase and decrease to constant of curves. The values of Young's modulus for ZnO thin films are also listed in Table 1.

Nanoscratch Testing

Figures 3(a–c) show wear track appearance for ZnO thin films deposited on a-axis sapphire, c-axis sapphire, and (0001) 6H-SiC substrates, respectively. Fig. 3(a) displays a shallow wear track surface, whereas Fig. 3(b, c) show a deeper wear track surface. It is important to note that ZnO/a-axis sapphire has lower surface roughness and higher hardness while its μ remain at lower levels and comparable to those of the rest two thin films.

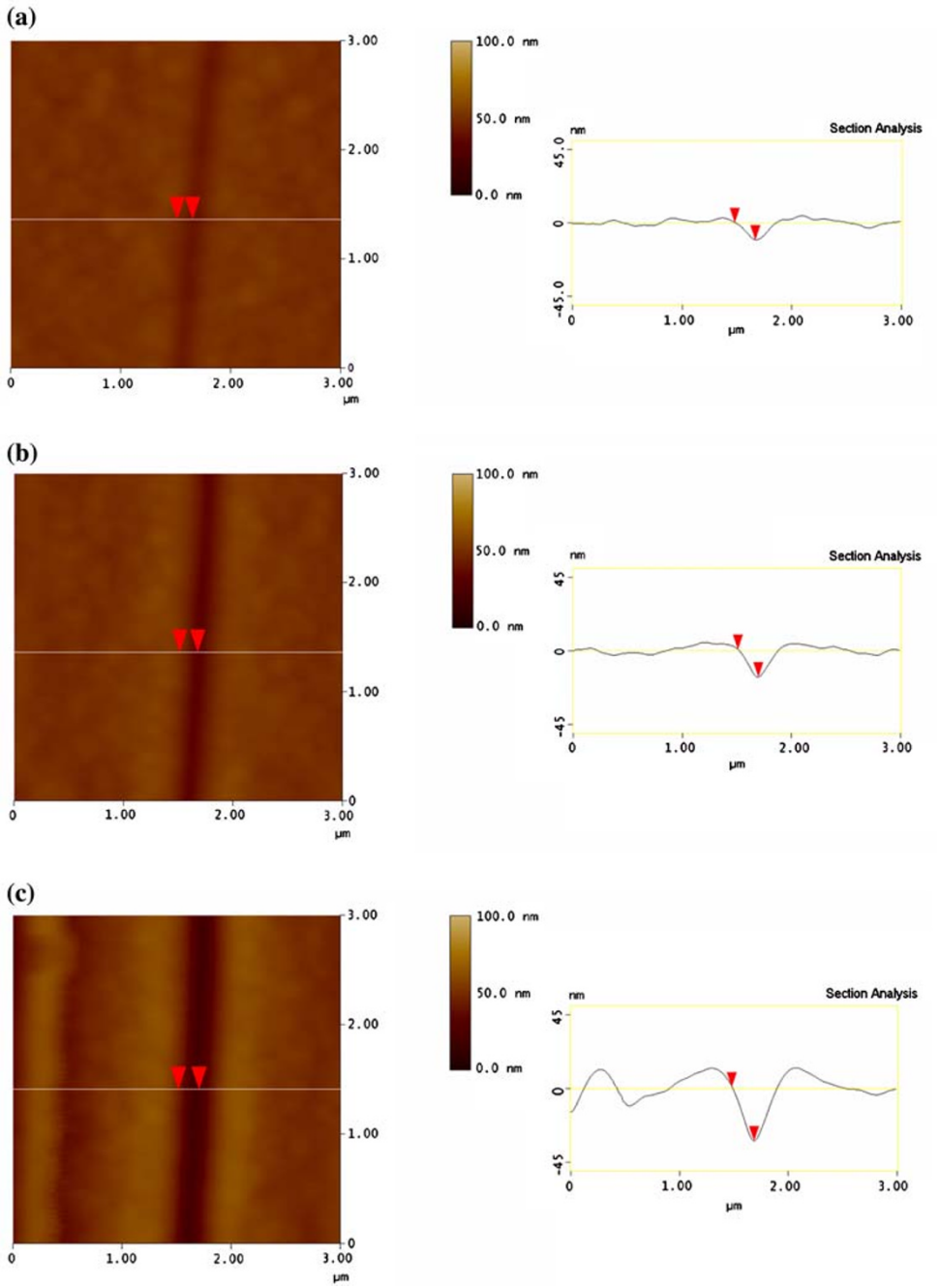

Fig. 3 AFM images and cross-sectional high profiles of scratches made at a normal load of 5 mN on ZnO thin films deposited on (**a**) a-axis sapphire, (**b**) c-axis sapphire, and (**c**) (0001) 6H-SiC substrates

Figure 4 is a plot of the friction coefficient (μ) versus scratch length (normal load). The μ is calculated by taking the ratio of the lateral force and the normal load on the indenter [31]. The fluctuation in the friction coefficient values is promoted by point-on orientation of the tip or the layered structure of thin films or it could be owing to nanoscale fracture events. The evolution of μ values shows small fluctuations and corresponds to mild wear, without any evidence of catastrophic damage or delamination of thin films. It was observed that increasing the normal load from 0.02 to 5 mN, μ was almost constant into early period (0.25 ± 0.02, 0.28 ± 0.01, 0.31 ± 0.02 for three different substrates are displayed in Fig. 4 and Table 1) despite the increase of the plastic deformation of ZnO thin films with the load, which resulted in grooving during scratch. In the meanwhile, the relationship between μ with scratch length (normal loading) almost was as well. No cracking of thin films took place, as also verified by our AFM observations while executing constantly 5 mN scratching loading each specimen, as illustrated in Fig. 3. In addition, the degree of

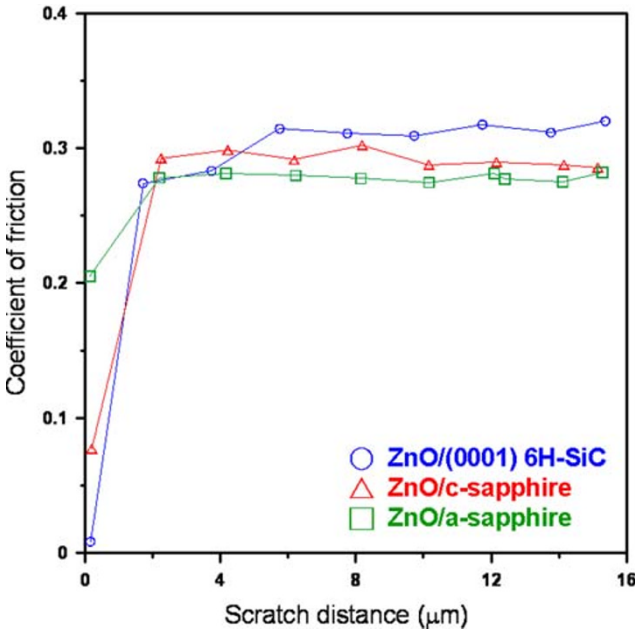

Fig. 4 Coefficient of friction as a function of the scratch distance under the normal load from 0.02 to 5 mN for three different samples

pile-up phenomenon across the residual profile can be obtained by AFM; in particular more manifest at the end of the scratch length each specimen.

In addition, hardness to Young's modulus ratio (H/E_{film} ratio) is a key parameter determining the type of behavior observed in nanoindentation and nanoscratch [32], i.e., this ratio can be regarded as a tool to describe values for performance criteria which are important to define the wear resistance of materials, such as the critical yield pressure for plastic deformation, the elastic strain to failure and the fracture toughness. Therefore, a high H/E_{film} ratio is often a reliable indictor of good wear resistance in materials [33]. The values are listed in Table 1. Results indicated that the best H/E_{film} ratio is displayed at ZnO thin film deposited on a-axis sapphire substrate.

Conclusion

We report in this article structural features and nanomechanical characterizations of ZnO thin films deposited on various substrates by the PLD system using AFM and nanoindentation techniques, while the nanoscratch resistance and frication coefficients are investigated by analyzing the scratching processes of thin films.

Results indicate that the hardness of ZnO thin films: 11.5 ± 0.8, 7.4 ± 0.1, and 5.9 ± 0.2 GPa for a-axis sapphire, c-axis sapphire, and (0001) 6H-SiC substrates, respectively. On the other hand, the highest Young's modulus of 212.5 ± 0.1 GPa appear at the a-axis sapphire substrate, while the lowest one of 117.1 ± 0.4 GPa at (0001) 6H-SiC. In addition, the smoother surface roughness and, a relatively lower friction coefficient equal to approximately 0.25 ± 0.02 and long wear life are also displayed at ZnO thin film deposited on a-axis sapphire substrate. No delamination and evidence of all ZnO thin films failure are observed in the present scratch tests.

Acknowledgment This work was partially supported by the National Science Council of Taiwan and I-Shou University, under Grant No.: NSC 97 – 2218-E-214-003, NSC 96-2221-E492-007-MY3 and ISU97-07-01-04.

References

1. D.C. Look, J.W. Hemsky, J.R. Sizelove, Phys. Rev. Lett. **82**, 2552 (1999)
2. A. Tsukazaki, M. Kubota, A. Ohtomo, T. Onuma, K. Ohtani, H. Ohno, S.F. Chichibu, M. Kawasaki, Jpn. J. Appl. Phys. **44**, L643 (2005)
3. G. Beshkov, G.P. Vassilev, M.R. Elizalde, T.G. Acebo, Mater. Chem. Phys. **82**, 452 (2003)
4. X.D. Li, H. Gao, C.J. Murphy, K.K. Caswell, Nano Lett. **3**, 1495 (2003)
5. X. Tao, X. Wang, X.D. Li, Nano Lett. **7**, 3172 (2007)
6. C.H. Chien, S.R. Jian, C.T. Wang, J.Y. Juang, J.C. Huang, Y.S. Lai, J. Phys. D: Appl. Phys. **40**, 3985 (2007)
7. S. Ruffell, J.E. Bradby, J.S. Williams, Appl. Phys. Lett. **89**, 091919 (2006)
8. E. Le Bourhis, G. Patriarche, Micro. **38**, 377 (2007)
9. S.R. Jian, Nanoscale Res. Lett. **3**, 6 (2008)
10. B. Bhushank, X.D. Li, Inter. Mater. Rev. **48**, 125 (2003)
11. B. Bhushan (ed.), *Springer Handbook of Nanotechnology* (Springer, Heidelberg, Germany, 2004)
12. G. Wei, B. Bhushan, N. Ferrell, D. Hansford, J. Vac. Sci. Technol. A **23**, 1856 (2005)
13. A. Tsukazaki, A. Ohtomo, T. Onuma, M. Ohtani, T. Makino, M. Sumiya, K. Ohtani, S.F. Chichibu, S. Fuke, Y. Segawa, H. Ohno, H. Koinuma, M. Kawasaki, Nature Mater. **4**, 42 (2005)
14. K. Ip, Y.W. Heo, D.P. Norton, S.J. Peatron, J.R. LaRoche, F. Ren, Appl. Phys. Lett. **85**, 1169 (2004)
15. K. Miyoshi, Y.W. Chung, *Surface Diagnostics in Tribology: Fundamental Principles and Applications* (World Scientific Publishing, Singapore, 1993)
16. D. Cáceres, I. Vergara, R. González, E. Monroy, F. Calle, E. Muñoz, F. Omnès, J. Appl. Phys. **86**, 6773 (1999)
17. X.D. Li, B. Bhushan, Mater. Charact. **48**, 11 (2002)
18. W.C. Oliver, G.M. Pharr, J. Mater. Res. **7**, 1564 (1992)
19. P.F. Yang, H.C. Wen, S.R. Jian, Y.S. Lai, S. Wu, R.S. Chen, Microelectron. Reliab. **48**, 389 (2008)
20. C. Charitidis, Y. Panayiotatos, S. Logothetidis, Diamond Relat. Mater. **12**, 1088 (2003)
21. S.O. Kucheyev, J.E. Bradby, J.S. Williams, C. Jagadish, M.V. Swain, Appl. Phys. Lett. **80**, 956 (2002)
22. J.E. Bradby, S.O. Kucheyev, J.S. Williams, C. Jagadish, M.V. Swain, P. Munroe, M.R. Phillips, Appl. Phys. Lett. **80**, 4537 (2002)
23. S.J. Bull, J. Phys. D: Appl. Phys. **38**, R393 (2005)
24. I. Zarudi, J. Zou, L.C. Zhang, Appl. Phys. Lett. **82**, 874 (2003)
25. G. Patriarche, F. Glas, G.L. Roux, L. Largeau, A. Mereuta, J.L. Benchimol, J. Cryst. Growth **221**, 12 (2000)
26. S. Brochard, J. Rabier, J. Grillhe, Eur. Phys. J. AP. **2**, 99 (1998)

27. V.A. Coleman, J.E. Bradby, C. Jagadish, P. Munroe, Y.W. Heo, S.J. Pearton, D.P. Norton, M. Inoue, M. Yano, Appl. Phys. Lett. **86**, 203105 (2005)
28. S. Zhao, Y. Zhou, Y. Liu, K. Zhao, S. Wang, W. Xiang, Z. Liu, P. Han, Z. Zhang, Z. Chen, H. Lu, K. Jin, B. Cheng, G. Yang, Appl. Surf. Sci. **253**, 726 (2006)
29. R. Navamethavan, K.K. Kim, D.K. Hwang, S.J. Park, J.H. Hahn, T.G. Lee, G.S. Kim, Appl. Surf. Sci. **253**, 464 (2006)
30. X.D. Li, H.S. Gao, C.J. Murphy, L.F. Gou, Nano Letters **10**, 1903 (2004)
31. T.W. Scharf, J.A. Barnard, Thin Solid Fillms **308–309**, 340 (1997)
32. A. Leyland, A. Mattews, Wear **246**, 1 (2000)
33. W. Ni, Y.T. Cheng, M. Lukitsch, A.M. Weiner, L.C. Lev, D.S. Grummon, Wear **259**, 842 (2005)